Environmental Research Letters

Plants as sensors: vegetation response to rainfall predicts root-zone water storage capacity in Mediterranean-type climates

David N Dralle[1], W Jesse Hahm[2], Daniella M Rempe[3], Nathaniel Karst[4], Leander D L Anderegg[5], Sally E Thompson[6], Todd E Dawson[7] and William E Dietrich[8]

[1] Pacific Southwest Research Station, United States Forest Service, Davis, CA, United States of America
[2] Department of Geography, Simon Fraser University, Burnaby, BC, Canada
[3] Jackson School of Geosciences, University of Texas at Austin, Austin, TX, United States of America
[4] Division of Mathematics and Science, Babson College, Wellesley, MA, United States of America
[5] Department of Integrative Biology, University of California at Berkeley, Berkeley, CA, United States of America
[6] Civil, Environmental, and Mining Engineering, The University of Western Australia, Perth, Australia
[7] Department of Integrative Biology, University of California at Berkeley, Berkeley, CA, United States of America
[8] Earth and Planetary Sciences, University of California at Berkeley, Berkeley, CA, United States of America

E-mail: david.dralle@usda.gov

OPEN ACCESS

RECEIVED
6 May 2020

REVISED
2 August 2020

ACCEPTED FOR PUBLICATION
20 August 2020

PUBLISHED
6 October 2020

Keywords: root-zone water storage capacity, seasonally dry, evapotranspiration, stochastic

Abstract

In Mediterranean-type climates, asynchronicity between energy and water availability means that ecosystems rely heavily on the water-storing capacity of the subsurface to sustain plant water use over the summer dry season. The root-zone water storage capacity (S_{max} [L]) defines the maximum volume of water that can be stored in plant accessible locations in the subsurface, but is poorly characterized and difficult to measure at large scales. Here, we develop an ecohydrological modeling framework to describe how S_{max} mediates root zone water storage (S [L]), and thus dry season plant water use. The model reveals that where S_{max} is high relative to mean annual rainfall, S is not fully replenished in all years, and root-zone water storage and therefore plant water use are sensitive to annual rainfall. Conversely, where S_{max} is low, S is replenished in most years but can be depleted rapidly between storm events, increasing plant sensitivity to rainfall patterns at the end of the wet season. In contrast to both the high and low S_{max} cases, landscapes with intermediate S_{max} values are predicted to minimize variability in dry season evapotranspiration. These diverse plant behaviors enable a mapping between time variations in precipitation, evapotranspiration and S_{max}, which makes it possible to estimate S_{max} using remotely sensed vegetation data — that is, using plants as sensors. We test the model using observations of S_{max} in soils and weathered bedrock at two sites in the Northern California Coast Ranges. Accurate model performance at these sites, which exhibit strongly contrasting weathering profiles, demonstrates the method is robust across diverse plant communities, and modes of storage and runoff generation.

1. Introduction

Measuring and predicting spatial variations in critical zone (the CZ, Earth's 'dynamic skin' (Grant and Dietrich 2017), extending from the vegetation canopy down to fresh bedrock) architecture is a challenging earth science research frontier (Riebe *et al* 2017, Pelletier *et al* 2016, Fan *et al* 2019). One CZ property central to understanding the ecohydrological function of landscapes is the capacity for the subsurface to store water that can be used by ecosystems. This property can be quantified as the root-zone water storage capacity, S_{max} [L] (de Boer-Euser *et al* 2016, Dawson *et al* 2020), defined as the volume of subsurface void space available to store water that can be accessed by vegetation, per unit ground area (Klos *et al* 2018). Physically, S_{max} is constrained by the depth and extent of weathering in the CZ, in conjunction with the depth of the active root zone (e.g. Hahm *et al* 2019b).

In rain-dominated seasonally dry or drought-prone regions, the only source of water available to plants during extended dry periods is that which is stored and available to root systems in the subsurface. The capacity of the subsurface to store this water therefore (i) regulates plant water use and productivity, impacting the Earth's near-surface energy budget and climate, and (ii) mediates water balance

partitioning, including runoff responses to rainfall during wet periods, and baseflow production during dry periods. These outcomes have been extensively explored in Mediterranean climates, where water delivery via precipitation and energy delivery through insolation are out of sync, so that dry season water use and productivity are almost completely constrained by the availability of water carried over from the wet season in soil, rock moisture, snowpack, and groundwater (Hahm *et al* 2019a, Graham *et al* 2010, Rempe and Dietrich 2018, Klos *et al* 2018, Garcia and Tague 2015, Hahm *et al* 2019b, Lewis and Burgy 1964, Zwieniecki and Newton 1996, Arkley 1981, Anderson *et al* 1995, Rose *et al* 2003, Smettem *et al* 2013, Eliades *et al* 2018, Enzminger *et al* 2019, Peel *et al* 2007). Given this, appropriate representations of the root-zone water storage capacity are urgently needed for use in novel large-scale modeling frameworks (Fan *et al* 2019) and in the range of existing modeling and empirical frameworks that rely on the concept of root-zone water storage capacity (Porporato *et al* 2004, Seyfried *et al* 2009). However, while maps of near-surface soil and its water storage properties exist (Geza and McCray 2008, Entekhabi *et al* 2010), information on whole-CZ subsurface properties, including water storage capacity in deep (>2m) soils, saprolite and weathered bedrock, is generally lacking at large spatial scales. For example, soil maps that are widely used to parameterize land surface and hydrological models not only rely on interpolation between sparsely spaced soil pits (Natural Resources Conservation Service 2019), but are generally confined to shallow depths (<2m) that do not cover the entire root zone.

Some methods exist to infer root-zone water storage capacity based on plant optimality principles (e.g. plants 'set' S_{max} so as to maximize productivity (Speich *et al* 2018, Yang *et al* 2016, Cabon *et al* 2018)), or variations in subsurface water storage inferred either through mass balance or remote sensing of terrestrial water storage. Storage-deficit approaches (Gao *et al* 2014, Wang-Erlandsson *et al* 2016) isolate accumulated evapotranspiration during dry periods to place lower bounds on S_{max}, although these methods typically assume vegetation themselves determine S_{max} at a value sufficient to overcome droughts with a specific, user-defined return interval. Other forms of storage-tracking approaches require data from stream gauging stations (Hahm *et al* 2019a), which are often too sparsely distributed to allow findings to be reliably interpolated. Microwave-based satellite observations of soil moisture storage dynamics are extensive but coarsely resolved and limited to shallow near surface soils (Entekhabi *et al* 2010). Space-based gravity observations (Swenson *et al* 2003) and ground-based surface deformation (Argus *et al* 2014, Enzminger *et al* 2019) are sensitive to changes in water storage, but only over extremely large spatial scales. These methods may also measure changes in water storage within deep aquifers which do not relate to changes within the root zone.

An alternative method to infer S_{max} from observations is to use the plants themselves as sensors of water availability, and therefore as windows into root-zone water storage dynamics (Thompson *et al* 2011, Thompson and Katul 2011). These 'inverse methods' (Wang-Erlandsson *et al* 2016) rely on the fact that plant productivity and water use are sensitive to both water and energy availability (Holdridge 1947, Stephenson 1990). Thus, if S_{max} determines how much water is stored and available to vegetation, S_{max} could potentially be inferred by inverting models of the rainfall-CZ-vegetation interactions using remotely sensed measures of vegetation activity and precipitation (Ichii *et al* 2009, Campos *et al* 2016, Kleidon 2004). In a more recent study, Hahm *et al* (2019a) demonstrated, via remote-sensing of plant greenness and water-balance tracking, that water storage properties of the CZ could decouple dry season water availability, and thus plant productivity, from year-to-year rainfall variability, suggesting that simplified statistical measures of evapotranspiration, such as its coefficient of variation, might also be diagnostic of root-zone water storage capacity.

Here, we expand on this collection of approaches by developing a simple stochastic model for root-zone water storage. The model introduces a simplified representation of ecohydrological seasonality within existing stochastic modeling frameworks (Zanardo *et al* 2012, Dralle and Thompson 2016, Feng *et al* 2015) to explicitly examine the dependence of S on intra-seasonal features of rainfall and S_{max}. We demonstrate that the model can be used as an inversion tool to infer S_{max}, given the basic premise that year-to-year variability in dry season plant water use should reflect year-to-year variability in root-zone water storage, manifested through the control of S_{max} on rainfall storage in the subsurface.

Using a remotely sensed ET dataset and empirical rainfall statistics, we find that the inversion accurately predicts S_{max} at two Eel River Critical Zone Observatory (ERCZO) field sites in the Northern California Coast Ranges where independent hillslope- and catchment-scale measurements of S_{max} have previously been made.

2. Methods

To understand how S_{max} mediates dry season water availability from year to year, we rely on a stochastic framework to predict the end-of-wet season root-zone water storage ($S_0 \in [0, S_{max}]$), the key variable which links wet season root-zone water storage dynamics to dry season water availability (figure 1(b)). We follow the formulations in Porporato *et al* (2004) and simulate wet season root-zone water storage ($S(t)$ [L]) using a 1-D, vertically integrated model

Table 1. Definition of terms used.

Term	Dimensions	Definition
S	L	root-zone water storage
S_{max}	L	root-zone water storage capacity
t	T	time
P	L T^{-1}	rainfall that enters the root zone
λ	T^{-1}	rainfall event frequency
α	L	mean depth of rainfall in an event
ET	L T^{-1}	evapotranspiration losses from the root zone
ET_{dry}	L	evapotranspiration loss from the root zone in dry season
PET	L T^{-1}	wet season average potential evapotranspiration
ET_{max}	L T^{-1}	maximum allowable evapotranspiration rate from the root zone
D	L T^{-1}	drainage from root zone
n	-	porosity
Z_r	L	root-zone depth
θ	-	volumetric water content
s	-	relative water content
s_{wp}	-	relative water content at wilting point
s_{fc}	-	relative water content at field capacity
T_{wet}	T	duration of wet season
T_{dry}	T	duration of dry season
$C_{2.5}$, $C_{97.5}$	T	days on which 2.5 and 97.5 percent, respectively, of cumulative annual rain falls in an average composite year

(illustrated in figure 1), where the governing mass balance can be expressed as:

$$\frac{dS}{dt} = P(t) - ET[S(t)] - D[S(t), P(t)]. \quad (1)$$

P [L/T] is rainfall entering the root zone, ET [L/T] represents evapotranspiration losses from the root zone, and D [L/T] represents drainage from the root zone. S is defined as the volume of water (expressed as a depth of liquid water) stored in the root zone that is accessible to vegetation, which ranges from 0, representing a wilting point, to S_{max}, the previously defined root-zone water storage capacity. Evapotranspiration increases linearly from zero at $S = 0$ to a maximum allowable evapotranspiration (ET_{max}, which we approximate with potential evapotranspiration, PET) at $S = S_{max}$. PET is assumed to be constant and equal to its average value during the rainy season. On daily timescales, rainfall volumes entering the root zone that would increase storage above S_{max} are instantaneously removed by drainage (D), so that S is always less than or equal to S_{max}. We note that S and S_{max} can be expressed in terms of typical parameters in simple soil moisture models (e.g. Porporato *et al* 2004): a relative soil moisture (s) equal to volumetric water content (θ) divided by porosity (n), a root-zone depth (Z_r), a field capacity s_{fc}, and a wilting point s_{wp}, such that $S_{max} = nZ_r(s_{fc} - s_{wp})$ and $S = nZ_r(s - s_{wp})$. Although mathematically equivalent to the model presented by Porporato *et al* (2004), the formulation here is expressed in terms of S (as opposed to a relative soil moisture, s) to highlight the fact that plant accessible water need not be restricted to soils; S may include storage within unsaturated saprolite and weathered bedrock. Vegetation access to water in the saturated zone is not considered within this framework.

2.0.1. Seasonal rainfall as a stochastic process

Wet season rainfall is modeled as a stochastic Poisson process (Milly 1993, Porporato *et al* 2004, Good *et al* 2017), assuming rainfall events occur at random with frequency λ [T^{-1}]. Due to the properties of Poisson processes, the inter-arrival times between rainfall events can be described with an exponential probability density function with mean $1/\lambda$ [T]. Upon the occurrence of a rainfall event, the event depth (volume of fallen rain per unit area) is also described using an exponential distribution with mean α [L]. The average seasonal rainfall is therefore equal to the product of α, λ, and the length of the wet season, T_{wet}. Rainfall seasonality is assumed to be binary, with no rainfall during the dry season, and stationary hydroclimatic features (constant α, λ, and ET_{max}) during the wet season.

2.0.2. Seasonality and running the model

Porporato *et al* (2004) found a steady-state solution for equation (1) under stationary climate conditions, and showed that the root-zone water storage follows a truncated gamma probability distribution (such that S is greater than zero and less than or equal to S_{max}). However, to our knowledge, unsteady, stochastic formulations of equation (1), such as the model formulated here, cannot be solved in closed form. Other

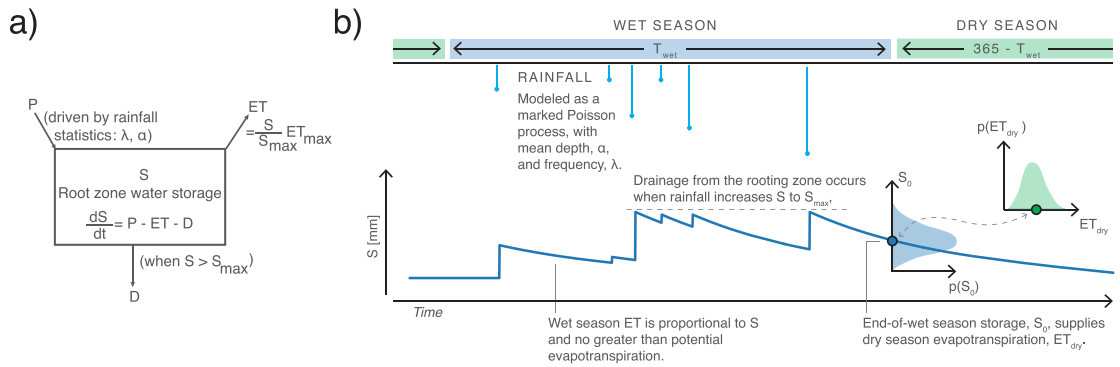

Figure 1. Stochastic root-zone storage model. 1-D root-zone box model (a) with the water balance equation and relevant fluxes. A single illustrative wet season (b) root-zone water storage trace is shown (dark blue line). Storage rises rapidly in response to rain events (light blue vertical lines on upper axis) and declines slowly due to evapotranspiration in between rain events. The realized end-of-wet season water storage, S_0 (filled blue circle), is one of many possibilities, whose mean and standard deviation are represented by the probability density function $p(S_0)$. S_0 determines (and is assumed to be directly proportional to) the amount of dry season evapotranspiration (filled green circle).

authors have found approximate solutions for certain types of seasonality (Feng *et al* 2015), but to avoid error potentially associated with such approximations, we opt to solve the governing equation using Monte Carlo simulations (for implementation details, see code availability statement).

2.1. Role of dry season evapotranspiration (ET_{dry}) for predicting S_{max}

We wish to infer root-zone water storage capacity, S_{max}, as a function of hydroclimate and vegetation water use. The model takes values of S_{max} to map wet season hydroclimate to S_0, which is not easily measured or observed. We therefore exploit the fact that in winter-wet summer-dry climates, the more readily observable magnitude of ET_{dry} typically will scale linearly with S_0 (Feng *et al* 2017). That is, dry season water use will increase proportionally with the storage condition at the end of the wet season. While we do not explicitly model ET_{dry}, it will equal $S_0 - S_0 \exp(-S/S_{max} \cdot ET_{max} \cdot T_{dry}) = S_0\left(1 - \exp(-S/S_{max} \cdot ET_{max} \cdot T_{dry})\right)$, where T_{dry} is the duration of the dry season (365 - T_{wet}). The final equality shows that the volume of water evapotranspired during the dry season is proportional to dry season initial storage (S_0), which in turn is set by the stochastic realization of that year's wet season rainfall. This relationship between observable plant water use and root-zone storage dynamics is a key linkage that we leverage in the following section to infer subsurface CZ storage properties.

As a simplifying assumption, the model uses a zero root-zone storage condition ($S = 0$) at the start of the wet season. This is reasonable if dry season rainfall is negligible, and if root-zone water storage declines exponentially over the dry season as described above, such that end of summer S is small relative to S_0.

2.2. Model inversion for estimating S_{max}

Given the four hydroclimate parameters (T_{wet}, α, ET_{max}, λ), Monte Carlo simulations can be used to obtain wet season root-zone storage dynamics, including a distribution for S_0, for a range of values of S_{max}. This yields a function which maps the range of S_{max} to variability in S_0:

$$CV[S_0] = f(S_{max}). \tag{2}$$

Using the proportionality between ET_{dry} and S_0 described in the previous section ($ET_{dry} \propto S_0$), we can use simple statistical properties to link remotely observable evapotranspiration to model predictions of S_0 for a given S_{max} and hydroclimate. Specifically, linear proportionality between two random variables implies that their coefficients of variation are equal: $CV[ET_{dry}] = CV[S_0]$, where CV is the coefficient of variation, equal to the standard deviation divided by the mean. This implies that the two coefficients of variation can be used interchangeably to estimate relative variability in the other. This provides a method for using remotely sensed measures of dry season vegetation water use (ET_{dry}) as an indicator of subsurface storage dynamics. Specifically, an estimate of $CV[ET_{dry}]$ from satellite remote-sensing data can be substituted into equation (2) for $CV[S_0]$, which is more difficult to observe directly. An estimate of S_{max} can be obtained by inverting this relationship:

$$\begin{aligned} CV[S_0] = CV[ET_{dry}] = f(S_{max}) \\ \Rightarrow \quad S_{max} = f^{-1}(CV[ET_{dry}]). \end{aligned} \tag{3}$$

This method for estimating storage is more widely applicable than the flux-tracking methodology presented in Hahm *et al* (2019a), because it does not rely on closure of the water budget, and thus can be applied even where stream gauging is unavailable or stream hydrology is modified.

2.3. Case studies: model application and inversion at well-characterized field sites

To parameterize the stochastic model, we rely on hydroclimatic records from two study watersheds within the Eel River Critical Zone Observatory: Elder Creek (16.9 km^2) and Dry Creek (3.5 km^2). Intensive hillslope monitoring of hillslope hydrology, plant dynamics, and stream runoff has been ongoing at Elder Creek for roughly a decade (Salve *et al* 2012, Link *et al* 2014, Oshun *et al* 2016, Kim *et al* 2014, Hahm *et al* 2019b, Lovill *et al* 2018, Rempe and Dietrich 2018), and at Dry Creek since 2015 (Hahm *et al* 2018, Dralle *et al* 2018, Lovill *et al* 2018). The regional Mediterranean climate here has a warm summer dry season, followed by cool winter wet season (Peel *et al* 2007). Elder Creek receives approximately 2000 mm of annual precipitation, and Dry Creek approximately 1800 mm (PRISM Climate Group 2004), almost all of which falls as rain, primarily between November and April. Although it rains more at Elder Creek, the greater canopy cover (see below) results in more interception, and the amount of throughfall at both sites is similar (Hahm *et al* 2019b).

Both sites lie within the Franciscan Formation, an exhumed subduction complex that is locally comprised of three coast-parallel (roughly north-south) belts (Blake Jr and Jones 1974). The Elder Creek watershed is located in the westernmost Coastal Belt, which is comprised mostly of shale (argillite), with lesser components of sandstone and conglomerate (Jayko *et al* 1989, Salve *et al* 2012, Lovill *et al* 2018). The Dry Creek watershed is about 20 km to the southeast and is underlain by the Central Belt, which consists of mélange with an intensely sheared, primarily argillaceous matrix with coherent blocks of various lithologies, dominated by sandstone (Blake Jr and Jones 1974, Lovill *et al* 2018).

Despite the proximity and similar climates of the sites, their contrasting lithologies lead to dramatic differences in the depth of weathering and structure of the critical zone, and corresponding large differences in storage dynamics (Hahm *et al* 2019b). Hahm *et al* (2019b) demonstrate that lithologically-controlled differences in subsurface water storage explain the contrasting vegetation communities between the two sites: the limited depth of weathering at Dry Creek results in low root-zone water storage capacity, and correspondingly an oak savanna plant community typically associated with much lower rainfall climates, while the thick subsurface CZ at Elder Creek seasonally stores enough water to support dense evergreen forest. Dralle *et al* (2018) develop a mass-balance based approach to estimate volumes of seasonally dynamic water storage in the subsurface that do not generate pressure gradients that drive streamflow generation, and suggest that these water volumes may be representative of root-zone water storage. Rempe and Dietrich (2018) measure unsaturated, root-zone water storage in weathered, fractured rock and saprolite at the Elder Creek site, demonstrating that this rock moisture supplies the vast majority (up to 300 mm) of transpiration water during the protracted dry season. Collectively, these studies provide multiple independent estimates of $S_{\max}$ (100-200 mm at Dry Creek, and 300-400 mm at Elder Creek; mostly within weathered bedrock below soils) that can be used to evaluate the results of the stochastic modeling framework.

2.3.1. Data

Daily rainfall volumes are measured with tipping bucket rain gauges at the ERCZO weather stations, and are corrected for wind-induced undercatch and interception (see Dralle *et al* 2018 for details). Although the Poisson rainfall model assumes that rainfall event occurrences are independent in time, rainfall events are often temporally autocorrelated along the California coast (Müller *et al* 2014). Therefore, we define a rainfall event as any consecutive period of days with non-zero rainfall, with a total event depth equal to the sum of rainfall over the consecutive period, and an occurrence date marked halfway through the event. Rainfall frequency λ is calculated as the total number of events divided by the length of the wet season (T_{wet}, calculated as described below), and α is calculated as the average of all event depths. $ET_{\max}$ is set equal to average daily potential evapotranspiration (PET) over the wet season. We compute daily PET (the same at both sites) using Eel River CZO weather station data and the Hargreaves equation (Hargreaves and Samani 1985):

$$ET_{\max} = PET = 0.002\,3 \cdot (T_{mean} + 17.8)\,(T_{\max} - T_{\min})^{0.5} \cdot 0.408 \cdot R_{ext}, \quad (4)$$

where $T_{\max}$, $T_{\min}$, T_{mean} are the daily max, min, and mean air temperatures, and R_{ext} is extraterrestrial solar radiation computed from latitude and day of year following (Allen *et al* 1998). We choose this particular model for *PET* due to its simplicity and its previous successful application at the two study sites (Dralle *et al* 2018).

We implement a new method to determine the length (T_{wet}) and boundaries of the wet season. First, we add the rain on each day of the year across all years (2001 to 2017) to collapse the rainfall record into a single composite representative year. Beginning in the heart of the dry season (August 1), we define the start of the wet season ($C_{2.5}$) as the day on which 2.5 percent of the cumulative rain has fallen in the composite representative year, and the end of the wet season ($C_{97.5}$) as the day on which 97.5 percent of the cumulative rain has fallen. The number of days between these dates ($(C_{97.5} - C_{2.5})$ defines T_{wet}. The selected cutoff values are subjective, and other definitions and methods for estimating wet season length yield similar results (e.g. Müller *et al* 2014, Dralle and Thompson 2016). The proposed method,

however, is advantageous for three reasons: 1) The slope of the cumulative rainfall distribution between the thresholds that emerges based on this definition is approximately linear (see acknowledgements for repository with supporting plots), consistent with the model requirement of stationary rainfall statistics, 2) This method allows the wet season length to vary on a site-by-site basis depending on local climatology, and 3) The algorithm is simple and readily applicable across large spatial scales. The four model parameters (λ, α, T_{wet}, and $ET_{\max}$) are reported in table 2.

During the dry season months of June, July, and August, negligible rain falls, and therefore variability in ET is likely attributable to variations in storage conditions. Estimates of actual evapotranspiration during these months are therefore used to compute $CV[ET_{dry}]$ to predict $S_{\max}$. ET_{dry} estimates are obtained from a biophysical evapotranspiration model (Breathing Earth System Simulator, BESS) that has been evaluated across California and FLUXNET sites globally (Ryu *et al* 2011, Baldocchi *et al* 2019, Jiang and Ryu 2016). The ET dataset used here is available from 2001 to 2017. Similar results were obtained using other *ET* datasets that are available at larger scales, such as the NASA/EOS MODIS global evapotranspiration product (Mu *et al* 2013). All 17 years of the Baldocchi *et al* (2019) ET dataset used in this study are freely available, and provided with the code required to replicate results at https://github.com/daviddralle/storage_cvs/.

2.3.2. Simulation exercises

We perform two simulation exercises; one to illustrate model output for a fixed climate and different $S_{\max}$, and a second to infer $S_{\max}$ from $CV[ET_{dry}]$ and explore the potential effects of changing rainfall statistics at the two case study sites.

2.3.2.1. Simulation exercise 1

In the first simulation exercise we use the model to illustrate seasonal patterns of wetting for three different values of $S_{\max}$, holding wet season length and climate statistics constant. Thirty years are simulated for each case to illustrate controls on S_0 and its interannual variability. This reveals how S_0 and its relative variability ($CV[S_0]$) depend on $S_{\max}$ and the specific occurrence and depth of rainfall events.

2.3.2.2. Simulation exercise 2

The second simulation first computes $CV[S_0]$ across a range of values of $S_{\max}$ for the hydroclimatic parameters in table 2. We use the resulting relationship between $CV[S_0]$ and $S_{\max}$ ($CV[S_0] = f(S_{\max})$) outlined in section 2.2, along with estimates of dry season evapotranspiration variability, to predict $S_{\max}$ at the two study sites. This procedure is equivalent to finding the mathematical inverse of the function f. We then compare these predictions to independently determined field-based estimates of $S_{\max}$. We additionally illustrate how changes in rainfall frequency (λ) and intensity (α) might alter the relationship between $S_{\max}$ and $CV[S_0]$.

Table 2. Empirical model parameters calculated for the study sites. The same parameters are used at both Dry Creek and Elder Creek (see Site Descriptions).

Parameter	Value
T_{wet} [days]	224 (Oct 4 to May 15)
$ET_{\max}$, wet season [mm/day]	1.88
λ, wet season [1/day]	0.11
α, wet season [mm]	71.0

3. Results

3.1. Simulation exercise 1

Figure 2 depicts Monte Carlo simulation of wet season root-zone water storage for different values of $S_{\max}$ using the parameters in table 2. Note that in all three panels an equivalent *absolute* moisture loss from the root zone results in different *relative* declines in S because $S_{\max}$ varies in each case.

In figure 2(a), because the root-zone storage capacity is small relative to the mean annual rainfall, S reaches $S_{\max}$ early in the season (grey line traces of individual yearly simulations reach the top of the plot). However, for the same reason, wet season evapotranspiration between rain events rapidly draws down the limited storage, causing S to deviate from and return to $S_{\max}$ many times throughout the wet season. These deviations, relative to the mean value of S_0, are large in this first case. The value of S_0 in any given year is most sensitive to the timing and magnitude of late wet season rainfall events, as demonstrated by the red and blue traces, where a late pulse of rainfall accounts for elevated S_0 in the blue trace relative to the red trace.

In contrast, in figure 2(c), $S_{\max}$ is large relative to the mean annual rainfall. Moreover, S does not reach $S_{\max}$ in many simulated years, resulting in highly variable S_0. However, because evapotranspiration depletes the large storage reservoir more slowly than in figure 2(a) (smaller inter-event declines in S), S_0 variability is controlled by *total* wet season rainfall rather than the pattern and properties of rainfall events at the end of the wet season.

Figure 2(b) reveals an intermediate case, in which $S_{\max}$ is small enough relative to rainfall so that $S_{\max}$ is reached in almost all years, but large enough that S is not significantly reduced (in a relative sense) during rainless periods. This leads to a low value for $CV[S_0]$, and the annual value of S_0 being relatively insensitive to both the total amount of wet season rainfall and the timing and magnitude of rain events toward the end of the wet season.

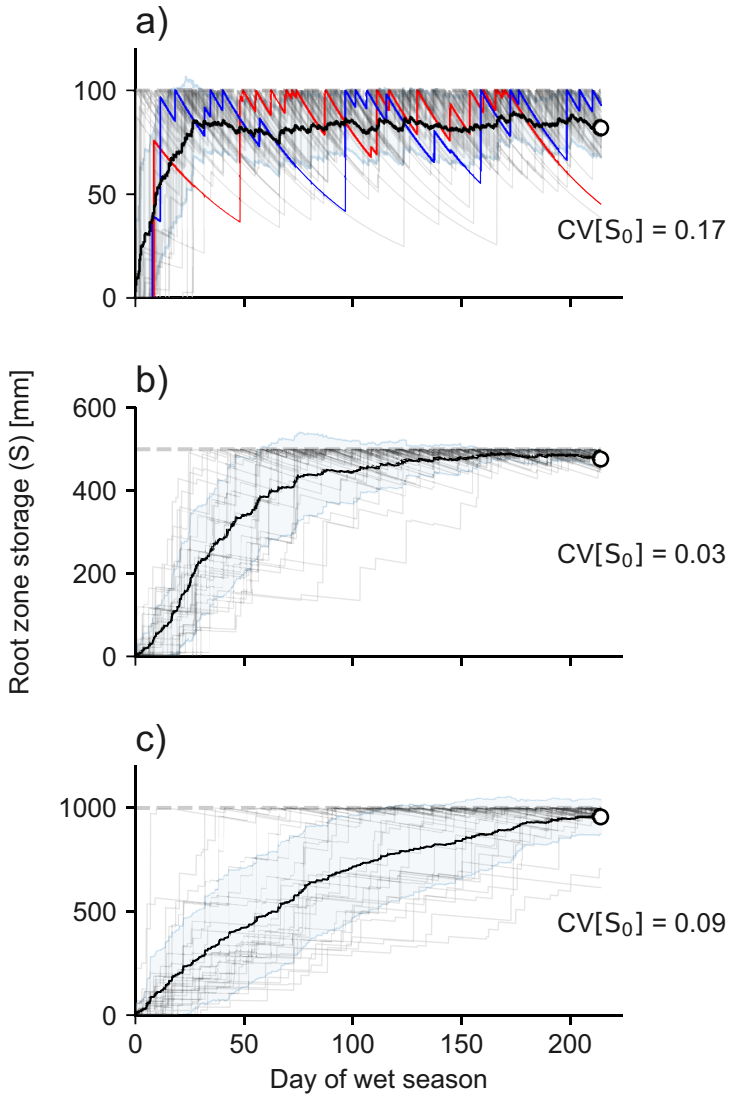

Figure 2. Root-zone water storage dynamics for increasing S_{max} (illustrated with the horizontal dashed line; 100 mm (a), 500 mm (b), and 1000 mm (c)). Note absolute differences in vertical scales. Thirty Monte Carlo realizations of model storage output are plotted in light gray traces for each case. The seasonal progression of the ensemble mean is denoted with a bold black line, with a start-of-dry season value (the mean of S_0) shown with a black point. Light blue envelopes represent plus or minus one standard deviation about the mean. Red and blue traces in (a) demonstrate that for small S_{max}, high S_0 variability is largely explained by rainfall patterns toward the end of the wet season, not total annual rainfall.

3.2. Simulation exercise 2

In the second exercise, we run Monte Carlo simulations of the model with ERCZO hydroclimatic parameters (table 2) to obtain theoretical estimates of $CV[S_0]$ (that is, the CV of the end of wet season root-zone storage in the simulations in figure 2) for values of S_{max} ranging from 0 to 1000 mm (figure 3(a)). Note that the CV values differ slightly between figures 2 and 3(a) for values of S_{max} equal to 100, 500, and 1000 mm. This is because the number of simulated years in figure 2 is limited to 30 for illustrative purposes, and so the estimated value of CV has not converged to the theoretical, limiting value presented in figure 3(a). As described in Methods (see section 2.2), figure 3(a) also graphically depicts the inversion procedure used to estimate S_{max}, with predicted values of 184 mm at Dry Creek, and 303 mm at Elder Creek. Inferred volumes of root-zone water storage capacity compare well with direct, independent estimates from the two sites. Using downhole neutron probes and soil time domain reflectometry, Rempe and Dietrich (2018) estimate that the seasonal change in vadose zone water content (which we interpret as S_{max}) at Elder Creek is between 300 and 400 mm. Dralle *et al* (2018) used wells to estimate S_{max} at Dry Creek between 120 and 200 mm.

Whereas figure 3(a) plots $CV[S_0]$ for single, constant values of α and λ representative of the ERCZO, figure 3(b) illustrates how the relationship between S_{max} and $CV[S_0]$ would change for shifts in the frequency and magnitude of rainfall events. Increases or decreases in α and λ have different effects on this relationship. A 50% decrease in storm frequency ($\lambda_{-50\%}$) or intensity ($\alpha_{-50\%}$) leads to a universal increase in

$CV[S_0]$. The magnitude of increase is much greater for larger values of S_{max}, and the increase is globally more sensitive to decreases in λ than decreases in α. Similarly, increases in storm frequency ($\lambda_{+50\%}$) lead to a larger drop in $CV[S_0]$ compared to increases in intensity ($\alpha_{+50\%}$). As with $\alpha_{-50\%}$ and $\lambda_{-50\%}$, increases in frequency or magnitude have a greater effect for larger values of S_{max}.

3.3. Resolving the non-uniqueness in the inversion procedure

Values of S_{max} computed through the inversion procedure are not unique in figure 3 because the theoretical curve $CV[S_0]$ vs. S_{max} is not monotonic. Figure 2 reveals graphically why this non-monotonic behavior arises: $CV[S_0]$ is minimized at an intermediate value of S_{max}. The minimum is also clearly identified in figure 3 near $S_{max} \approx 600$ mm. Far left of this minimum, S_{max} is small and so $CV[S_0]$ increases because late wet season ET can rapidly deplete S, which may or may not be replenished by rainfall in the final weeks of the wet season. Far right of the minimum, $CV[S_0]$ begins to increase because larger S_{max} increases sensitivity of S_0 to variations in total wet season precipitation. This suggests that if ET_{dry} is insensitive to total wet season rainfall, the inversion procedure should map to the left of the minimum on the modeled curve in figure 3. To verify the figure 3 inversions, we regress ET_{dry} at both sites onto wet season precipitation (figure 4), finding statistically insignificant (p values greater than 0.05) slopes of 0.002 at Dry Creek and -0.016 at Elder Creek (that is, 100 mm of additional rainfall would result in 0.2 mm and -1.6 mm change in dry season evapotranspiration at Dry Creek and Elder Creek, respectively), consistent with the findings of Hahm *et al* (2019a). We therefore conclude the two sites likely fall to the left of the minimum in figure 3, mapping to smaller values of S_{max} that are in agreement with independent field estimates.

4. Discussion

A reduced complexity stochastic model for root-zone water storage dynamics in Mediterranean climates demonstrates that plant response to climatic variability can be used to estimate root-zone water storage capacity in the critical zone. At two rain-dominated sites in Northern California with strongly contrasting weathering profiles, model predictions closely match direct measurements of storage capacity in shallow soils and underlying weathered bedrock.

4.1. Limitations of the modeling approach

A novel contribution of this paper is the development and validation of a relatively simple and widely applicable method in Mediterranean climates to determine root-zone water storage capacity, a key ecohydrological parameter. However, the method is only strictly valid in rain-dominated Mediterranean regions, and where fixed properties of the CZ (such as porosity profiles), rather than potentially plastic properties (such as highly variable root zone extents), determine S_{max}. Future work will focus on development of more general methods that can be applied to more diverse climates.

A second limitation of the method is the reliance on remotely sensed measures of vegetation water use. We used a biophysical evapotransipiration model (Breathing Earth System Simulator) for evapotranspiration, presented for California in Baldocchi *et al* (2019), which importantly does not include any specific representation of the subsurface. Other evapotranspiration models which explicitly incorporate soil water balance modeling for ET estimation should not be used for the method presented here (Martens *et al* 2017), because they make assumptions regarding the size of S_{max}, which this approach estimates. By using ET data (Baldocchi *et al* 2019) that relies primarily on remotely sensed spectral signatures, this method may struggle in places where plant functional group phenology undergoes minimal change across a range of transpiration rates. This should be explored further, but we note that at the sites we studied, as is the case in much of California, there is large seasonal phenological variation (Hahm *et al* 2019a). One other potentially confounding factor in our analysis is the extent to which year-to-year variation in summer energy supply might impact dry season plant water use. Because plants across California are typically water-limited rather than energy-limited in the summer dry season (i.e. PET greatly exceeds ET), this is unlikely to matter, as Hahm *et al* (2019a) found.

Finally, the model representation of subsurface water runoff and storage dynamics is highly simplified. All rainfall is assumed to infiltrate, such that no Horton overland flow occurs, limiting the scope of the model's applicability. We are also uncertain as to whether deeper root profiles, such as those observed in the Elder Creek watershed (from previous drilling and neutron probe campaigns (Salve *et al* 2012, Rempe and Dietrich 2018, Hahm *et al* 2019b)), can be usefully modeled within a framework that treats the entire vadose zone as a homogeneous reservoir. Within riparian areas or low-lying areas, or in areas with shallow root depths or thin subsurface critical zones, water table dynamics in the near surface may play an important role in setting S_{max}. Although plants do not explicitly use water from the saturated zone in the model, the Dry Creek catchment provides some evidence that where field capacity does not greatly differ from saturation (Dralle *et al* 2018), the model still may be useful, and likely still improves estimates of root-zone water storage capacity relative to existing soil datasets.

4.2. Ecosystem sensitivity to climate

Understanding drivers of ecosystem sensitivity to climate is important for understanding the

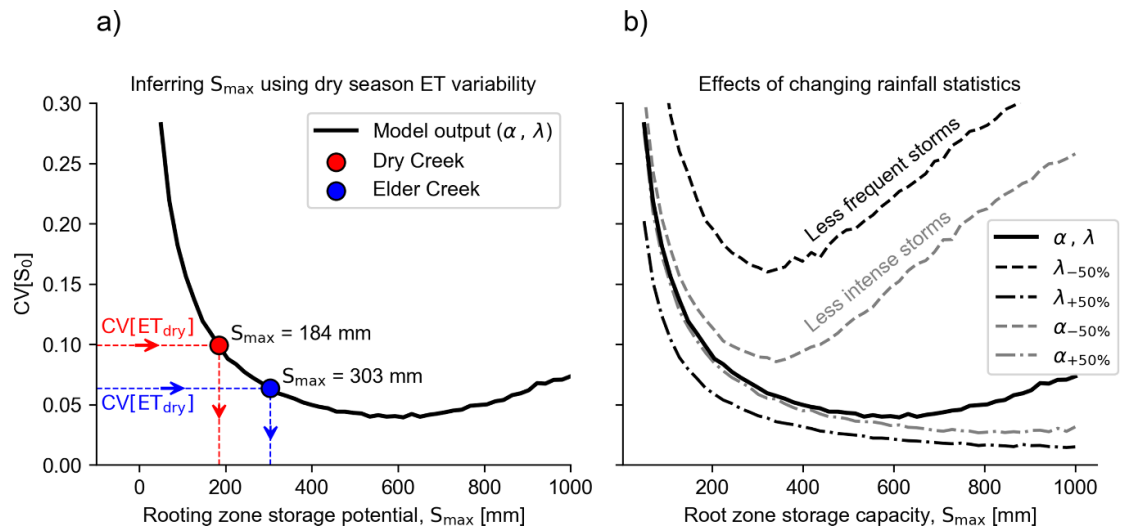

Figure 3. A graphical demonstration of the procedure used to estimate S_{max} at the study locations. In (a) S_{max} is inferred from dry season ET variability ($CV[ET_{dry}]$), based on the relationship between S_{max} and $CV[S_0]$. The inference is made possible by equating the more readily measurable $CV[ET_{dry}]$ with $CV[S_0]$. Measured values of $CV[ET_{dry}]$ ($= CV[S_0]$) are plotted for Elder (blue) and Dry Creek (red) on the y-axis. The dashed lines with arrows graphically depict the inversion procedure, whereby S_{max} is estimated via intersection with the x-axis. Inferred values of S_{max} agree well with independently measured S_{max} for these sites. (b) Illustration of changes in the relationship $CV[S_0]$ and S_{max} for 50% decreases or increases in storm frequency ($\lambda_{-50\%}$ and $\lambda_{+50\%}$, respectively) or storm intensity ($\alpha_{-50\%}$ and $\alpha_{+50\%}$, respectively).

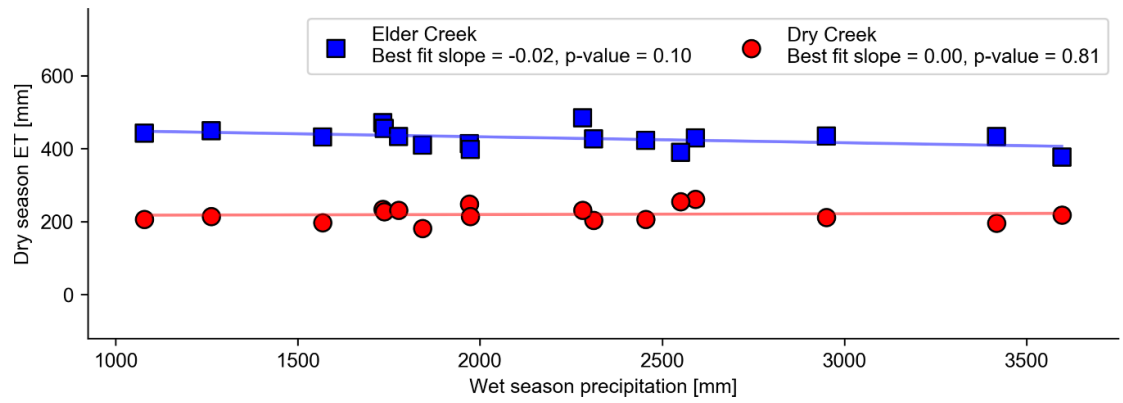

Figure 4. Dry season evapotranspiration plotted against wet season precipitation on equal scale axes for the Elder Creek and Dry Creek catchments.

impacts of climate change on global hydrologic and biogeochemical cycles. Here, we focused on how S_{max} might control dry season water availability and hence productivity. We demonstrate that dependence of water use on root-zone water storage capacity is more nuanced than is traditionally assumed. Too large or too small S_{max} — relative to annual rainfall — tends to increase the sensitivity of ET_{dry} to rainfall variability, with sensitivity minimized at intermediate values of S_{max}. This Goldilocks-like result differs from other modeled findings, which suggest increasing S_{max} monotonically increases plant water stress due to chronically low water content in the vadose zone (Porporato *et al* 2004, Zanardo *et al* 2012). These studies, however, did not consider the transient effects of seasonality.

Globally, rainfall patterns in many Mediterranean climate zones are predicted to change dramatically (Swain *et al* 2018, Valdes-Abellan *et al* 2017, Viola *et al* 2016, Feng *et al* 2019), though in distinct ways in different regions. In California for example, although mean annual rainfall is not predicted to change significantly, precipitation variability and event magnitudes are expected to increase (Swain *et al* 2018). In contrast, mean annual rainfall totals are predicted to decrease significantly throughout the European Mediterranean climate region (Gao and Giorgi 2008). The model presented here suggests that root-zone storage capacity plays an important role in determining how vegetation might respond to these varied trends. For example, the thin grey line traces in figure 2(a) show that at locations with low S_{max} relative to annual rainfall totals, late wet season rainfall patterns

seem to control annual variations in ET_{dry}, and thus presumably productivity. In such watersheds, shifts in intra-seasonal rainfall patterns, such as increased event magnitudes, may significantly alter dry season water availability. In contrast, the model predicts that relatively large values of S_{max} increase vegetation sensitivity to total rather than intra-seasonal dynamics of precipitation (figure 2(c)). Locations with intermediately sized S_{max} (relative to typical values of annual rainfall) may be least sensitive to increases in rainfall volatility (figure 2(b)). Figure 3(b) further illustrates these nuances, demonstrating that decreases in total rainfall (either through decreases in λ or α) may universally increase variability in productivity, likely due to the more frequent occurrence of years where S is not constrained by S_{max}; that is, the effective size of S_{max} *relative* to typical annual rainfall totals increases. This is supported by the observation that $CV[S_0]$ is more sensitive to rainfall decreases for larger values of root-zone storage capacity. Generally, vegetation in the present modeling framework is more sensitive to changes in rainfall frequency (λ) than to changes in the intensity of events (α), especially in the case where rainfall decreases ($\lambda_{-50\%}$ or $\alpha_{-50\%}$). This finding suggests that resolving whether projected decreases in rainfall are due to changes in frequency or intensity may be particularly important for predicting plant response to climate in drying regions.

5. Conclusion

We developed an ecohydrological model for Mediterranean climates that elucidates how root-zone water storage capacity and intra-annual rainfall patterns determine the sensitivity of plant water use to rainfall variability. By assuming that dry season plant water use, measured using a biophysical evapotranspiration model forced with remote sensing data (Ryu *et al* 2011, Baldocchi *et al* 2019), scales with the amount of root-zone water storage at the end of the wet season, we predict root-zone water storage capacity, an important yet presently challenging parameter to map. We validated the predictions with independent field-based estimates of S_{max} at two sites in the Northern California Coast Ranges. Our work demonstrates the potential for using remotely sensed ecohydrologic datasets paired with simple, process-based ecohydrological models to infer properties about the critical zone, including deeper weathered bedrock below shallow soils. Future efforts will be most fruitful if they can be validated with hillslope-scale subsurface observations, motivating greater observatory-style exploration of the critical zone across lithologic, climatic, and tectonic gradients.

Acknowledgment

We acknowledge support from the National Science Foundation CZP EAR-1331940 for the Eel River Critical Zone Observatory. The data and code (written in Python) required to reproduce the analyses and figures in this study are available at https://github.com/daviddralle/storage_cvs/.

References

Allen R G, Pereira L S, Raes D and Smith M 1998 Crop evapotranspiration-guidelines for computing crop water requirements-fao irrigation and drainage paper 56 *FAO, Rome* **300** D05109

Anderson M A, Graham R C, Alyanakian G J and Martynn D Z 1995 Late summer water status of soils and weathered bedrock in a giant sequoia grove *Soil Science* **160** 415–22

Argus D F, Fu Y and Landerer F W 2014 Seasonal variation in total water storage in california inferred from gps observations of vertical land motion *Geophys. Res. Lett.* **41** 1971–80

Arkley R J 1981 Soil moisture use by mixed conifer forest in a summer-dry climate 1 *Soil Sci. Soc. Am. J.* **45** 423–7

Baldocchi D, Dralle D, Jiang C and Ryu Y 2019 How much water is evaporated across california?: A multi-year assessment using a biophysical model forced with satellite remote sensing data *Water Resources Res.* **55** 2722–41

Cabon A, Martínez-Vilalta J, Martínez de Aragón J, Poyatos R and De Cáceres M 2018 Applying the eco-hydrological equilibrium hypothesis to model root distribution in water-limited forests *Ecohydrology* **11** e2015

Campos I, Gonzalez-Piqueras J, Carrara A, Villodre J and Calera A 2016 Estimation of total available water in the soil layer by integrating actual evapotranspiration data in a remote sensing-driven soil water balance *J. Hydrol.* **534** 427–39

Clark Blake Jr M and Jones David L 1974 Origin of franciscan melanges in Northern California *SEPM Special Publication* **19** 345–57

Dawson T E, Jesse Hahm W and Crutchfield-Peters K 2020 Digging deeper: what the critical zone perspective adds to the study of plant ecophysiology *New Phytologist* **226** 666–71

Dralle D N, Jesse Hahm W, Rempe D M, Karst N J, Thompson S E and Dietrich W E 2018 Quantification of the seasonal hillslope water storage that does not drive streamflow *Hydrol. Process.* **32** 1978–92

Dralle D N and Thompson S E 2016 A minimal probabilistic model for soil moisture in seasonally dry climates *Water Resour. Res.* **52** 1507–17

Eliades M, Bruggeman A, Lubczynski M W, Christou A, Camera C and Djuma H 2018 The water balance components of mediterranean pine trees on a steep mountain slope during two hydrologically contrasting years *J. Hydrol.* **562** 712–24

Entekhabi D *et al* 2010 The soil moisture active passive (smap) mission *Proc. IEEE* **98** 704–16

Enzminger T L, Small E E and Borsa A A 2019 Subsurface water dominates sierra nevada seasonal hydrologic storage *Geophys. Res. Lett.* **46** 11993–2001

Fan Y *et al* 2019 Hillslope hydrology in global change research and earth system modeling *Water Resources Research*

Feng X, Dawson T E, Ackerly D D, Santiago L S and Thompson S E 2017 Reconciling seasonal hydraulic risk and plant water use through probabilistic soil–plant dynamics *Global change biology* **23** 3758–69

Feng X, Porporato A and Rodriguez-Iturbe I 2015 Stochastic soil water balance under seasonal climates *Proc. R. Soc.* A **471** 20140623

Feng X, Thompson S E, Woods R and Porporato A 2019 Quantifying asynchronicity of precipitation and potential evapotranspiration in mediterranean climates *Geophys. Res. Lett.* **46** 14692–701

Gao H, Hrachowitz M, Schymanski S J, Fenicia F, Sriwongsitanon N and Savenije H H G 2014 Climate controls how ecosystems size the root zone storage capacity at catchment scale *Geophys. Res. Lett.* **41** 7916–23

Gao X and Giorgi F 2008 Increased aridity in the mediterranean region under greenhouse gas forcing estimated from high resolution simulations with a regional climate model *Glob. Planet. Change* **62** 195–209

Garcia E S and Tague C L 2015 Subsurface storage capacity influences climate–evapotranspiration interactions in three western united states catchments *Hydrol. Earth System Sci.* **19** 4845–58

Geza M and McCray J E 2008 Effects of soil data resolution on swat model stream flow and water quality predictions *J. Environ. Management* **88** 393–406

Good S P, Moore G W and Miralles D G 2017 A mesic maximum in biological water use demarcates biome sensitivity to aridity shifts *Nat. Ecol. Evolution* **1** 1883

Graham R, Rossi A and Hubbert R 2010 Rock to regolith conversion: Producing hospitable substrates for terrestrial ecosystems *GSA Today* **20** 4–9

Grant G E and Dietrich W E 2017 The frontier beneath our feet *Water Resour. Res.* **53** 2605–9

Hahm W J, Dralle D N, Rempe D M, Bryk A B, Thompson S E, Dawson T E and Dietrich W E 2019a Low subsurface water storage capacity relative to annual rainfall decouples mediterranean plant productivity and water use from rainfall variability *Geophy. Res. Lett.* **46** 6544–53

Hargreaves G H and Samani Z A 1985 Reference crop evapotranspiration from temperature *Applied Eng. Agriculture* **1** 96–9

Holdridge L R 1947 Determination of world plant formations from simple climatic data *Science* **105** 367–8

Ichii K, Wang W, Hashimoto H, Yang F, Votava P, Michaelis A R and Nemani R R 2009 Refinement of rooting depths using satellite-based evapotranspiration seasonality for ecosystem modeling in California *Agricultural Forest Meteorol.* **149** 1907–18

Jayko A S, Blake M C, McLaughlin R J, Ohlin H N, Ellen S D and Kelsey H M 1989 Reconnaissance geologic map of the covelo 30- by 60-minute quadrangle, Northern California *Report* 2001

Jesse Hahm W, Dietrich W E and Dawson T E 2018 Controls on the distribution and resilience of quercus garryana: ecophysiological evidence of oak's water-limitation tolerance *Ecosphere* **9** e02218

Jesse Hahm W, Rempe D M, Dralle D N, Dawson T E, Lovill S M, Bryk A B, Bish D L, Schieber J and Dietrich W E 2019b Lithologically controlled subsurface critical zone thickness and water storage capacity determine regional plant community composition *Water Resources Res.* **55** 3028–55

Jiang C and Ryu Y 2016 Multi-scale evaluation of global gross primary productivity and evapotranspiration products derived from breathing earth system simulator (bess) *Remote Sens. Environ.* **186** 528–47

Kim H, Bishop J K B, Dietrich W E and Fung I Y 2014 Process dominance shift in solute chemistry as revealed by long-term high-frequency water chemistry observations of groundwater flowing through weathered argillite underlying a steep forested hillslope *Geochim. Cosmochim. Acta* **140** 1–19

Kleidon A 2004 Global datasets of rooting zone depth inferred from inverse methods *J. Clim.* **17** 2714–22

Lewis D C and Burgy R H 1964 The relationship between oak tree roots and groundwater in fractured rock as determined by tritium tracing *J. Geophys. Res.* **69** 2579–88

Link P, Simonin K, Maness H, Oshun J, Dawson T and Fung I 2014 Species differences in the seasonality of evergreen tree transpiration in a mediterranean climate: Analysis of multiyear, half-hourly sap flow observations *Water Resour. Res.* **50** 1869–94

Lovill S M, Hahm W J and Dietrich W E 2018 Drainage from the critical zone: Lithologic controls on the persistence and spatial extent of wetted channels during the summer dry season *Water Resour. Res.* **54** 5702–26

Martens B, Miralles D G, Lievens H, Van Der Schalie R, De Jeu R A M, Fernández-Prieto D, Beck H E, Dorigo W and Verhoest N 2017 Gleam v3: Satellite-based land evaporation and root-zone soil moisture *Geoscientific Model Development* **10** 1903–25

Milly P C D 1993 An analytic solution of the stochastic storage problem applicable to soil water *Water Resour. Res.* **29** 3755–8

Mu Q, Zhao M and Running S W 2013 Modis global terrestrial evapotranspiration (ET) product (NASA mod16a2/a3) *Algorithm Theoretical Basis Document, Collection* **5**

Müller M F, Dralle D N and Thompson S E 2014 Analytical model for flow duration curves in seasonally dry climates *Water Resour. Res.* **50** 5510–31

Natural Resources Conservation Service. Web soil survey 2019

Oshun J, Dietrich W E, Dawson T E and Fung I 2016 Dynamic, structured heterogeneity of water isotopes inside hillslopes *Water Resour. Res.* **52** 164–89

Peel M C, Finlayson B L and McMahon T A 2007 Updated world map of the köppen-geiger climate classification *Hydrol. Earth Syst. Sci. Discussions* **4** 439–73

Pelletier J D, Broxton P D, Hazenberg P, Zeng X, Troch P A, Niu G-Y, Williams Z, Brunke M A and Gochis D 2016 A gridded global data set of soil, intact regolith and sedimentary deposit thicknesses for regional and global land surface modeling *J. Adv. Modeling Earth Syst.* **8** 41–65

Porporato A, Daly E and Rodriguez-Iturbe I 2004 Soil water balance and ecosystem response to climate change *The American Naturalist* **164** 625

PRISM Climate Group. Prism rainfall dataset 2004 (http://prism.oregonstate.edu)

Rempe D M and Dietrich W E 2018 Direct observations of rock moisture, a hidden component of the hydrologic cycle *Proc. Natl Acad. Sci.* **115** 2664–9

Riebe C S, Jesse Hahm W and Brantley S L 2017 Controls on deep critical zone architecture: a historical review and four testable hypotheses *Earth Surf. Process. Landf.* **42** 128–56

Rose K, Graham R and Parker D 2003 Water source utilization by pinus jeffreyi and arctostaphylos patula on thin soils over bedrock *Oecologia* **134** 46–54

Ryu Y *et al* 2011 Integration of modis land and atmosphere products with a coupled-process model to estimate gross primary productivity and evapotranspiration from 1 km to global scales *Global Biogeochem. Cycles* **25** GB4017

Salve R, Rempe D M and Dietrich W E 2012 Rain, rock moisture dynamics and the rapid response of perched groundwater in weathered, fractured argillite underlying a steep hillslope *Water Resour. Res.* **48** W11528

Seyfried M S, Grant L E, Marks D, Winstral A and McNamara J 2009 Simulated soil water storage effects on streamflow generation in a mountainous snowmelt environment, idaho, USA *Hydrol. Process.* **23** 858–73

Smettem K R J, Waring R H, Callow J N, Wilson M and Mu Q 2013 Satellite-derived estimates of forest leaf area index in southwest western australia are not tightly coupled to interannual variations in rainfall: implications for groundwater decline in a drying climate *Global Change Biol.* **19** 2401–12

Speich M J R, Lischke H and Zappa M 2018 Testing an optimality-based model of rooting zone water storage capacity in temperate forests *Hydrol. Earth System Sci.* **22** 4097–124

Stephenson N L 1990 Climatic control of vegetation distribution: the role of the water balance *Am. Naturalist* **135** 649–70

Swain D L, Langenbrunner B, David Neelin J and Hall A 2018 Increasing precipitation volatility in twenty-first-century California *Nat. Clim. Change* **8** 427

Swenson S, Wahr J and Milly P C D 2003 Estimated accuracies of regional water storage variations inferred from the gravity recovery and climate experiment (grace) *Water Resour. Res.* **39** 1223

Thompson S E, Harman C J, Troch P A, Brooks P D and Sivapalan M 2011 Spatial scale dependence of ecohydrologically

mediated water balance partitioning: A synthesis framework for catchment ecohydrology *Water Resour. Res.* **47** W00J03

Thompson S E and Katul G G 2011 Inferring ecosystem parameters from observation of vegetation patterns *Geophys. Res. Lett.* **38** 20

Valdes-Abellan J, Pardo M A and José Tenza-Abril A 2017 Observed precipitation trend changes in the western mediterranean region *Int. J. Climatol.* **37** 1285–96

Viola F, Francipane A, Caracciolo D, Pumo D, La Loggia G and Noto L V 2016 Co-evolution of hydrological components under climate change scenarios in the mediterranean area *Sci. Total Environ.* **544** 515–24

Wang-Erlandsson L *et al* 2016 Global root zone storage capacity from satellite-based evaporation *Hydrol. Earth Syst. Sci.* **20** 1459–81

Yang Y, Donohue R J and McVicar T R 2016 Global estimation of effective plant rooting depth: Implications for hydrological modeling *Water Resour. Res.* **52** 8260–76

Zanardo S, Harman C J, Troch P A, Rao P S C and Sivapalan M 2012 Intra-annual rainfall variability control on interannual variability of catchment water balance: A stochastic analysis *Water Resour. Res.* **48** W00J16

Zion Klos P *et al* 2018 Subsurface plant-accessible water in mountain ecosystems with a mediterranean climate *WIRES* **5** e1277

Zwieniecki M A and Newton M 1996 Seasonal pattern of water depletion from soil–rock profiles in a mediterranean climate in southwestern oregon *Canadian J. Forest Res.* **26** 1346–52

de Boer-Euser T, McMillan H K, Hrachowitz M, Winsemius H C and Savenije H H G 2016 Influence of soil and climate on root zone storage capacity *Water Resour. Res.* **52** 2009–24